Textile & Leather Review

ISSN 2623-6281 | www.tlr-journal.com | 10.31881/TLR

Multi-Parameter Analysis of Textile Materials

Yu Peng, Yangyang Min, Wei Dang, Haowen Shi, Zengbin Liu

How to cite: Peng Y, Min Y, Dang W, Shi H, Liu Z. Multi-Parameter Analysis of Textile Materials. Textile & Leather Review. 2024; 7:203-221. https://doi.org/10.31881/TLR.2023.146

How to link: https://doi.org/10.31881/TLR.2023.146

Published: 12 February 2024

Multi-Parameter Analysis of Textile Materials

Yu PENG[1]*,Yangyang MIN[2], Wei DANG[2], Haowen SHI[2], Zengbin LIU[2]

[1]School of Arts and Humanities, Hunan International Economics University, China

[2]College of Chemistry and Chemical Engineering, Yulin University, Yulin, Shaanxi 719000 China

*hongchen0410@126.com

Article

https://doi.org/10.31881/TLR.2023.146

Received 3 September 2023; Accepted 3 February 2024; Published 12 February 2024

ABSTRACT

Advanced constructions in the automotive, military, and aircraft sectors often employ textile materials. This is due to its advantageous mechanical characteristics, appealing supporting components, affordable manufacture, and simple handling. For architectural layout, textile composite analysis becomes crucial. It is costly and time-consuming to experimentally determine the rigidity and durability of textile materials. Due to the impossibility of disintegration, experimental testing can only provide the characteristics of a single textile layer. The disadvantage of a textile layer made up of various fibre orientations is that it is likely to display anisotropic physical performance. Based on the physical reaction of glass and epoxy resin materials, also the design of the textile materials, a multi-parameter (MP) analysis is used to identify the substance behaviour of textile materials via virtual testing. An estimate for just one layer or a whole textile prototype may be created using these simulated trials. Pressure-dependent and nonlinear responses of materials in the multi-parameter analysis are material models created especially for this purpose and are used to simulate. The simulations are contrasted with the outcomes of experimental tests, which reveal the properties of the textile materials. The findings stated that the proposed model has provided rigidity-dislocation of 0.30 in the simulation results.

KEYWORDS

multi-parameter analysis, textile, epoxy resin, glass, strength, flexibility, durability

INTRODUCTION

A great deal of attention must be paid to fibre identification to evaluate textile materials' performance, quality, and compositional qualities [1]. The procedure entails identifying the variety of the materials, including artificial, natural, and mixes of both, utilizing instruments such as sophisticated spectroscopic methods, chemical analysis, and microscopic inspection. Evaluating a material's mechanical properties, such as its tensile strength and abrasion resistance, is crucial to determining its strength and resistance to outside pressures [2]. For evaluating the degree of dyeing and the textile's ability to retain colour, tests for colourfastness and dye penetration are also conducted. The way a textile responds to different temperatures is another aspect of thermal analysis. It is critical to consider the complex interplay that happens between glass and epoxy resin components throughout this in-depth examination of fabrics [3]. The physical interaction between the component materials affects the physical properties of textile composites. Epoxy resin is widely recognized for its multifunctionality and

strong bonding characteristics. When epoxy resin is used with glassy materials, the interplay between the two becomes complex, requiring a thorough understanding to create structures that meet specific performance requirements [4]. However, conventional experimental techniques encounter certain constraints, specifically when it comes to assessing the rigidity and long-lasting properties of textile materials [5]. The aforementioned techniques frequently offer insights limited to the properties of an individual textile layer, hence failing to provide a holistic comprehension of material performance, encompassing non-linear and pressure-dependent reactions. The main rationale for adopting virtual testing is rooted in the need to address the inherent difficulties associated with empirically analyzing the many layers of textile materials. Traditional techniques are limited in their ability to offer comprehensive insights beyond the superficial layer [6]. The primary objective of our research is to investigate the complex interplay between the epoxy resin and glass components, with a particular emphasis on their physical interaction. The design of textile materials encompasses intricate arrangements and orientations of fibres, which have a significant impact on their performance [7]. To attain a state of equilibrium among strength, flexibility, and durability, it is imperative to comprehend their influence on the overall structural integrity of composites. Simulated trials are conducted to estimate the properties of individual layers as well as full textile prototypes while taking into account nonlinearity and pressure-dependent reactions [8]. The fascinating interaction of artistry and usefulness is seen in the field of textile design, where creativity and utility collide. A distinct viewpoint that defines textile design as more than merely a form of artistic expression arises within this dynamic field. In certain situations, textile design is intriguingly presented as a material imperfection, indicating a break from the traditional ideas of material perfection [9]. This comparison analysis attempts to establish a high level of dependability and accuracy by establishing a connection between the physical and virtual realms of material testing. The qualities that have been unveiled serve to enhance understanding of the development of sophisticated structures in industries such as automotive, military, and aerospace.

The researchers identified the top research focuses on employing textile materials for individual manufacturing in epidemic scenarios in light of the COVID-19 epidemic and the protective effect of medical textiles [10]. Results of a bibliographic portfolio including 16 studies that were relevant were obtained. The primary filtration mechanisms, cleaning techniques for N95 respirators, and suggested techniques for assessing the filtration effectiveness of various materials with potential for mask development are all included in this portfolio, which highlights the core emphasis of this study topic. Géczy et al. examined the effectiveness of commercially available, environmentally friendly textile materials for particle filtering using a quick, inexpensive, and effective mask validation approach [11]. Their findings fall short of the standard's stated depth and all-inclusive approach in every way. Krifa examined several well-known strategies and applications for creating smart textiles for wearable

technology [12]. In developing body-centric monitoring, the significance of flexible and electrically conductive fabrics is stressed. As an outcome, modern technology has been used in textile constructions to enable the integration of electrical components like sensors and systems for storing energy. Onggar et al. evaluated an overview of functional conducting polymers with a particular emphasis on how self-conducting, inherently conducting polymers might be combined to produce electrically conductive textile fabrics [13]. Different electrical textile devices may be made from the resultant conducting fibres and/or textile fabrics. Physicochemical sensors, thermoelectric fibres and textiles, heated clothing, artificial muscles, and textile supercapacitors are a few examples. To have enough information to forecast material properties and use this family of polymers in unique brands, additional study is still required. The medicine used for transdermal and topical skin treatments in clinical and medical settings has been examined [14]. This includes a description of the nature of human skin, the method for transdermal biologically active substances distribution, and the variables affecting delivery effectiveness. The resultant material composite has undergone testing for use in wound healing and skincare. Bartkowiak examined the produced elegant textile material by “shape memory alloys (SMAs)” resilience to heat variables like fires, molten metals, and radiant heat [15]. These findings support the use of smart clothes built from a framework containing SMA components even in situations where there is a high risk of exposure to thermal factors because it provides excellent protection for the outer layer and creates additional space when subjected to heat conditions, the user's skin lies between both the outer fabric and skin. The SMA components expanded as a result of the radiant heat flow, creating an air gap between the system's layers that measured around 13.3 mm. Machnowski identified the morphological and chemical changes brought on by heat radiation in four cotton/polyester mix textiles and their component fibres [16]. The results may also be used in science when it's essential to look at the evidence in the form of a textile item that has been exposed to heat radiation throughout the inquiry. The absorption/diffusion approach was used in the research to saturate textile materials incorporating copper-infused particles across the entirety of their material composition [17]. Consequently, after the completion of the treatment, the woollen textile samples exhibited the most elevated levels of copper-containing fragments. The design ideas and practical execution of a novel smart textile material may serve as the foundation for intensive care bedding and serve as a mobility sensor on its own [18]. According to these findings, the textile sheet is a highly sensitive pressure sensor that may continuously supply discriminating information to enable the extremely sensitive, in-the-moment detection of immobility. Kudzin focused on creating poly (lactide) nonwoven textiles that are both coated with and modified by the phosphoro-organic chemical [19]. These research findings demonstrate that bio-functionalized materials provide antimicrobial protection against a variety of bacterial pathogens. The most targeted antibacterial effect may be achieved by producing microcapsules with outer shells doped with silver nanoparticles [20]. It is

unknown how well textiles containing biologically active substances would heal these types of wounds. Tseghai stated that the methods for attaching conductive materials to and inside of a textile framework have been thoroughly reviewed [21]. The outcome showed how useful the recommended kHz-range sensors would be for developing a wearable device for moisture detection on textiles. Shin suggested a smart textile-composite actuator along with its use in a soft robotic gripper [22]. This resulted in a more pronounced gripping curve for the multi-layered construction. Therefore, this article aims to fill this research gap by employing a multi-parameter (MP) analysis as a virtual testing approach.

MATERIALS

Material imperfection implies that the mechanical properties of textile materials are very much dependent on the presence of material defects, particularly those found in textile design such as fibres and threads with diameters much smaller than the final composite framework. Utilizing a multi-parameter method, the influence of these microscopic defects on the macroscopic material performance is modelled. To comprehend and forecast the overall mechanical behaviour of the textile material, this method probably takes into account many aspects of fibres and yarns, including composition, structure, and arrangement. Microscale elements are employed to impart megascale material properties and characterise a textile's fibre strand structure. While micromechanical unit cells analyse the activity of the unidirectional (UD) material of the fibre strands, mid-mechanical unit cells are utilized to ascertain the material qualities of the fibre strands. Unit cells are utilized as a representative volume component in the micro and intermediate sizes. An elastic substance and plastic that is employed in micro and mid-scale structural unit cells is epoxy resin. An elastic substance and plastic that is employed in micro and mid-scale structural unit cells is epoxy resin. The laterally isotropic material paradigm for fibre bundles follows similar rules. Fibres are mimicked using a linear elastic material framework. The function of epoxy resin is significantly dependent on pressure, and it exhibits various stress-strain (SS) morphologies under compression, shear, and pressure. The substance, structure, organization and other material flaws found in textile design are all taken into account in this research which uses a multi-parameter approach, is to provide a more comprehensive knowledge of the performance of textile materials by capturing the intricate interactions between these parameters and their impact on their mechanical behaviour.

METHODOLOGY

Plastic-elastic method for epoxy resin

Under shearing, the epoxy resin shows remarkable ductile behaviour; nevertheless, under tension, it displays virtually brittle failure. It is decided to use a qualitative physical framework to clarify the nonlinearity of the substance up till collapse with plasticity. Plasticity thus describes material deterioration brought on by micro-cracks and viscoelastic processes. This is a feasible strategy since the experiments that follow will only utilize loads that increase uniformly. A quadratic yielding surface is presumed to be the best way to characterize the pressure-dependent activity. The yield region may be expressed in equation (1) about the initial 2 stress constants, pressure of hydrostatic$p$ and $VON\ MISES$stress ∂_{vm}^2.

$$Y = \partial_{vm}^2 - x_0 - x_1 P \tag{1}$$

where p is represented in equation (2)

$$P = \frac{1}{3}\partial_{ii}\text{and}\partial_{vm} = \sqrt{\frac{3}{2}sd_{ab}sd_{ab}} \tag{2}$$

The stress deviation vector is referred to as sd_{ab}. $VON\ MISES$ stress rvm is always favourable; however, the pressure of hydrostatic$p$ is optimistic for the hydrostatic strain and harmful for the hydrostatic contraction. Hardening lines are used to calculate the last two parameters, a0 and a1. The notation is used in equations (3) and (4) for hardening curves.

$$A_t = A_t\left(\bar{\varepsilon}^{Pl}\right) \tag{3}$$

$$A_s = A_s\left(\bar{\varepsilon}^{Pl}\right) \tag{4}$$

$$A_0 = 3\partial_s^2 \tag{5}$$

$$A_1 = 3\frac{\partial_t^2 - 3\partial_s^2}{\partial_t} \tag{6}$$

Equation (5) and (6) are used for calculating the parameters. As a result, the simulation accurately reproduces the test results that were collected practically. Based on the cumulative plastic strain epl, the yield stresses r_s and r_t are calculated using the hardening curves equation 3 at each time step. According to equation 1 for the quadratic yield function, other stress levels need to be taken into consideration. It must be emphasized that under pure hydrostatic pressure, this yield area does not

permit plastic movement. To prevent the volume expansion under pressure that happens when an integrated rate rule is employed in conjunction with the exponential yield surface, the route of movement is determined by a non-related flow rule. In equation (7), it is believed that the plastic capacity determines the pattern of non-associated flow.

$$C = \sqrt{o^2 + \propto P^2} \tag{7}$$

The bending-induced expansion or contraction of a substance's volume may be controlled by adjusting the flow component. Under uniaxial stress, the plastic Poisson's percentage mp is defined by equation (8).

$$u_p = \frac{8-3\propto}{16+3\propto} \Rightarrow \propto = \frac{8}{3}\frac{1-3u_p}{1+u_p} \tag{8}$$

When the hardening curves are entered as tabular data, the calculation may be handled simply without fitting into every analytical equation. This modelling does not require variable adjustment.

Degradation and softening of epoxy resin

Uni-axial elastic and compression forces are used to establish a quadratic breaking mode. The failure area is divided into two sections due to the need for the substance performance in pure shear to be taken into account as well. Therefore, there is no longer a need to do a lowest-squares fit on 2 parabolic variables using 3 input intensities; instead, all input intensities may be used directly. There is no failure under hydrostatic pressure since the parabolic failure zone extends in that direction. An analogous expression to the yielding area, which is specified in equation (9), exists for the failing substrate in the hydrostatic stress area when brittle tensile failure is considered.

$$R = \partial_{vm}^2 - B_0 - B_1 P \; for \; P > 0 \tag{9}$$

For r 14 0, the degradation criteria are met, and flexibility decline begins until substance breakdown occurs. The variables B_0 and B_1 are derived using the same method as the yield mechanism and the variables a0 and a1 are mentioned in equation (10). To replace the yield pressures in equation 10, one must use the structural capacities beneath the uni-axial tension (r_t) as well as shear (r_s). Contrary to the yielding stress, which varies throughout the hardening procedure, intensities are fixed values irrespective of other parameters; hence it must be observed that the failure area does not vary during modelling. It is feasible to define failure at various equal polymeric stresses for unique states of stress as yield and the failing area are not always the same at any point during the experiment. Degradation

under strain, for instance, happens sooner than failure under stress. Equation (11) assumes a continuous breakdown area linking the uniaxial tensile values r_c and the shear values r_s in the ∂_{vm} invariant plane, which is the area of hydrostatic pressure where ductility shear breakdown occurs. Equations (12) (13) (14) and (15) are the minimal equations used for determining the hydrostatic pressure obtained from stress states.

$$R = \partial_{vm} - B_2 - B_3 P \; for \; P < 0 \tag{10}$$

The B parameters are obtained from the following equations

$$B_0 = r_s^2 \tag{11}$$

$$B_1 = 3\frac{r_s^2 - r_c^2}{r_c} \tag{12}$$

$$B_2 = r_s \tag{13}$$

$$B_2 = 3\frac{r_s - r_c}{r_c} \tag{14}$$

$$\partial = (1 - d)\partial_{eff,} \tag{15}$$

Figure 1 shows that the fibre-matrix interaction is accurately modelled using a typical mesh. There are two meshes represented as 1(a) and 1(b). Figure 1a displays the original mesh created by ABAQUS, whereas Figure 1b depicts an updated mesh which includes only elements having an aspect proportion closer to one at the fibre-matrix interfaces. The damage progression in several meshes demonstrates the impact of irregularity elements which lead to mesh dependency. Figure 1 shows the results. Figure 1a demonstrates that the irregularity elements within the centre of the meshes operate as crack-stoppers, diverging a crack toward the interfaces. Figure 1b represents Damage that occurs along an interface of the updated mesh. Although mesh dependency is apparent in this simplistic geometry, manually producing regularity elements within sensitive regions is time-consuming and inefficient.

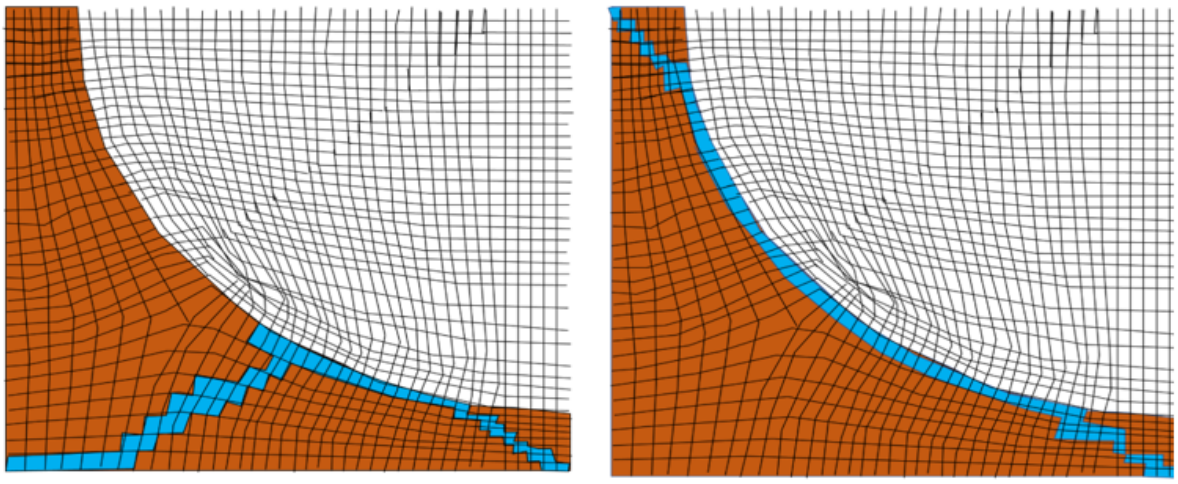

a) b)

Figure 1. a) Original mesh created by ABAQUS, b) Updated mesh with regularity elements along an interfaces

In the present study, voxel (volume pixel is referred to as voxel) meshing is employed, where every element has the identical size and aspect proportion of a single one. The material features subscribe to a previously defined mesh, resulting in an approximation meshing that doesn't take into consideration the actual geometry. The mesh-dependency is not present in voxel meshes, making them ideal for application through the fracture energies technique. Figure 2 depicts the damage progression with voxel meshes for the same stress situation as the normal meshes within Figure 1. Mesh refinements do not affect the crack's path as shown. Figure 2(a) represents the 30*30 elements and Figure 2(b) displays the 150*150 elements for damage progression beneath compressions.

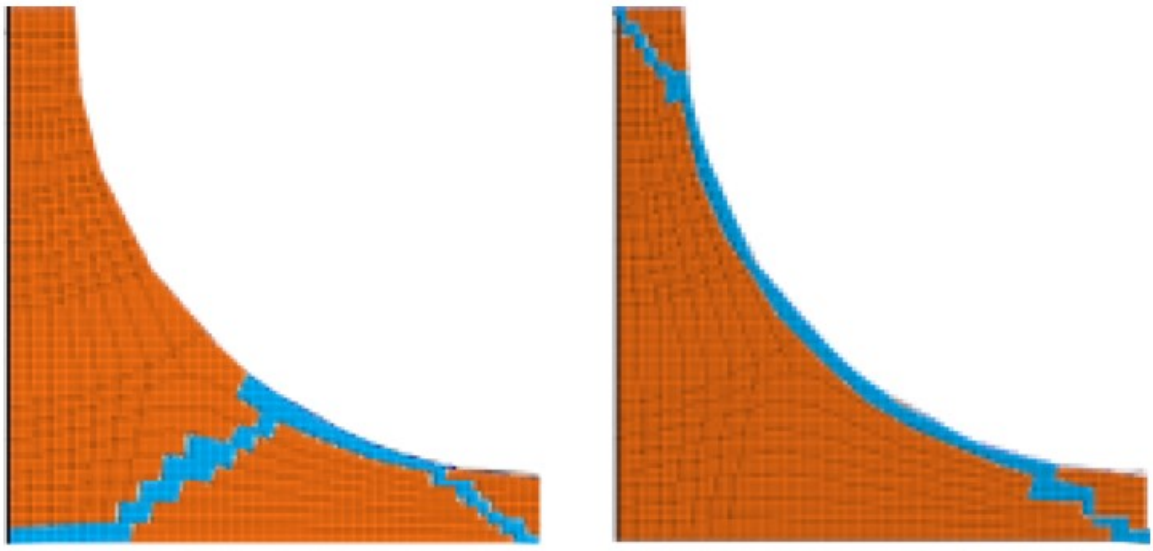

a) b)

Figure 2. a) 30*30 elements, b) 150*150 elements

RESULT AND DISCUSSION

In this section, the multi-parameter (MP) analysis results were discussed for textile materials. Stress-strain curves(SSC) unit cells of micromechanical under transverse and in-plane shear, mid-mechanical stress-strain lines in transverse and shear, load-dislocation, and rigidity-dislocation are among the characteristics utilized for the discussion.

Stress-strain curves of micromechanical unit

Micromechanical unit cell stress-strain curves under transverse pressure are shown in Figure 3, and those under in-plane shear are shown in Figure 4. Due to the excellent converging of peak usage and degradation strain, it is clear that the given substance and voxel mesh mixture perform extremely well. Local failure happens far in advance of the peak demand, leading to the conclusion that the percentage energy normalization substantially reduces mesh reliance. Static characteristics affect the differences after complete degradation, and they are unimportant for the compaction process. Table 1 demonstrates the findings for the stress and strain curve of transverse pressure and Table 2 depicts the SSC of in-plane shear.

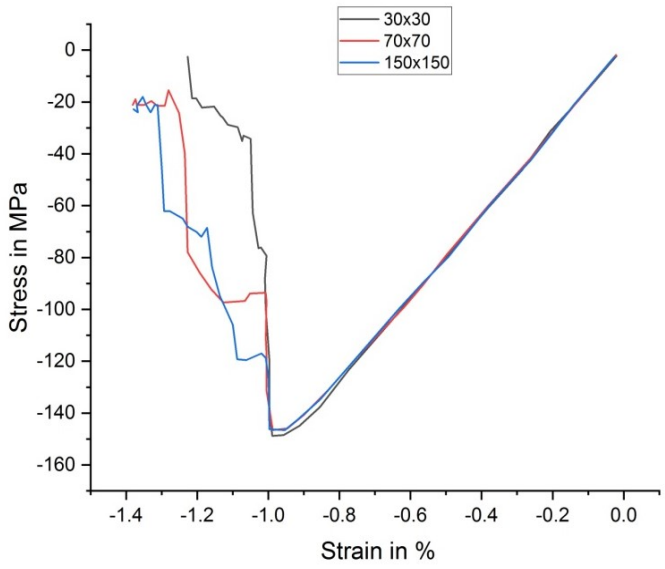

Figure 3. SSC of transverse pressure

Table 1. Results of the SSC of transverse pressure

Strain	Transverse pressure		
	30x30	70x70	150x150
-1.4	0	-20	-20
-0.8	-130	-130	-130
0	0	0	0

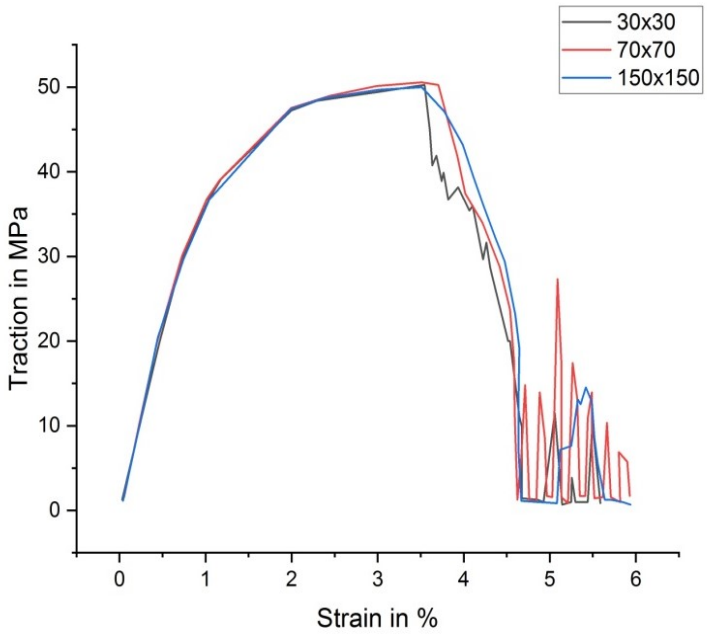

Figure 4. Stress-strain curve of in-plane shear

Table 2. Results of the SSC of in-plane shear

Strain	In-plane shear		
	30x30	70x70	150x150
2	40	40.1	40.3
4	28	31.1	34.1
6	0.6	1.5	0.8

A representative volumetric element (RVE) could be used to describe the behaviours of a layer by arranging the fibres and matrices. Perfectly periodic fibre configurations, such as squared and hexagonal, are frequently assumed, ignoring the random fibre distributions over the entire cross-section, as illustrated in Figure 5.

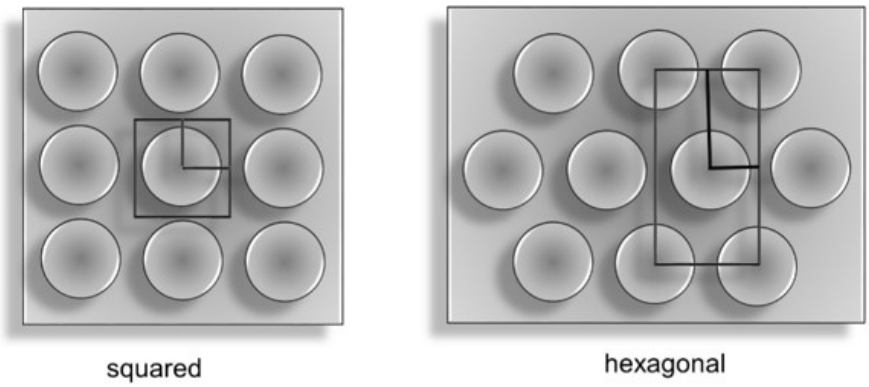

Figure 5. Hexagonal and squared configurations for micromechanical unit

Symmetrical load scenarios might decrease the unit cell to a fraction of the original size due to its symmetrical shape. Figure 6 depicts a squared unit cell with one-fourth of a fibre.

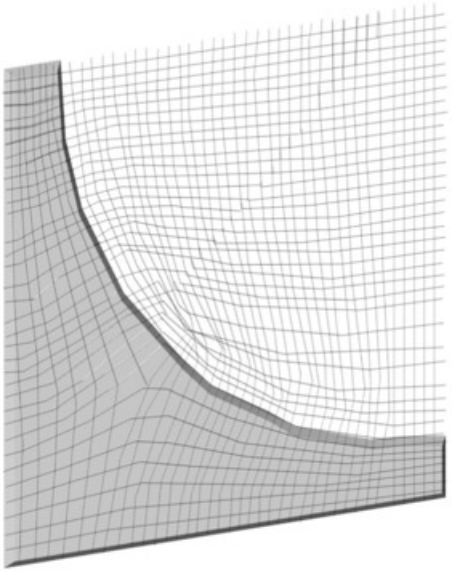

Figure 6. Discretization for one-fourth of the micromechanical unit

Stress-strain curves of mid-mechanical unit

Figures 7 and 8 depict the stress-strain curves of mid-mechanical cells during transversal compressions and in-plane shears, respectively. Table 3 illustrates the outcomes for the stress and strain curve of transverse pressure and Table 4 depicts the SSC of in-plane shear. With ordinary stresses, the material acts approximately linearly elastic till degradation, however, during shear, plastic deflections take place. These data may be compared since it is clear from the samples' cracked surfaces that intra-lamina degradation has a place. Since extremely unique samples' made of only one sheet with through-thickness reinforcing would need to be constructed to compare findings, this is not possible.

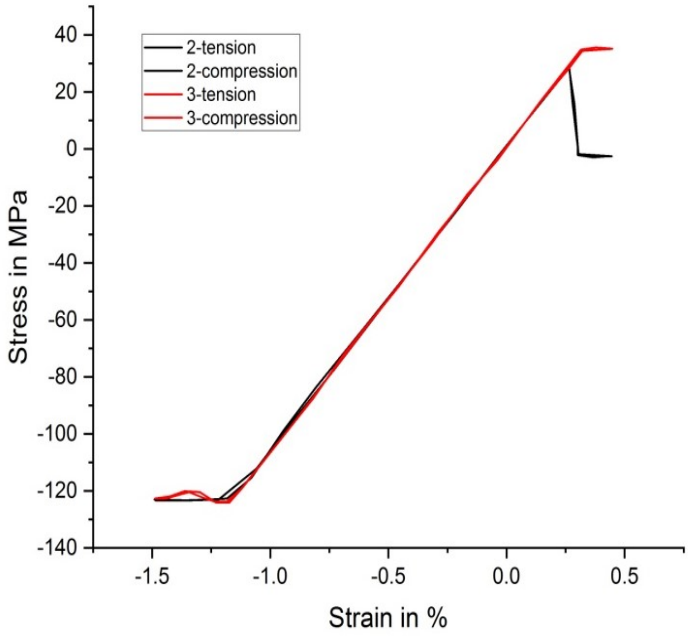

Figure 7. SSC of transverse pressure

Table 3. Results of SSC of transverse pressure

Strain	Transverse pressure	
	2-tension	2-compression
-1.5	-135	-135
-0.5	-60	-65
0.5	-10	-10

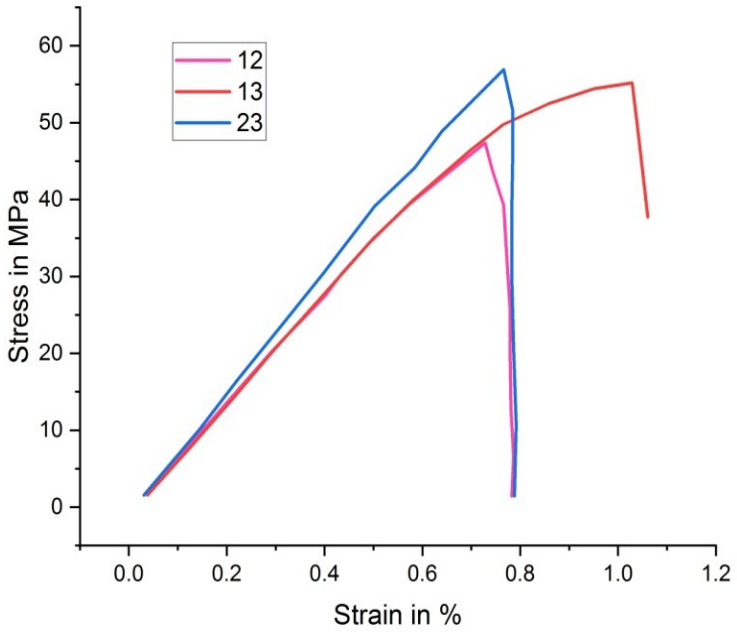

Figure 8. SSC of in-plane shear

Table 4. Results of the SSC of in-plane shear

Strain	In-plane shear		
	12	13	23
0.2	8.5	8.6	12
0.4	25.2	25.2	28.5
0.6	36.6	36.8	40

Figure 9(a) depicts a scanning for dry, un-impregnated, non-crimp textiles. The fabric's layout comprises 4 layers that are stacked in the following order: $[0^0/-45^0/90^0/45^0]$, having the top $0^0 - layer$ visible. Each layer has various thicknesses, with thickness fractions in $(48.7\%\ 0^0, 23.0\% - 45^0, 4.8\%\ 90^0, 23.0\%\ 45^0)$. Many unit cells have been designated on the dried textiles. A contrast of the designated regions indicates that the pattern's periodicity contains many imperfections.

Regarding the $45^0 - layers$, another unit cell shape could be preferable, however considering the broad spacing among the stitching and the large $0^0 - layer$ fibres fraction, this discrepancy might also be neglected. Figure 9(b) shows the discretization for the unit cells, which have 200 x 200 x 1 elements as well as employ a layer coordinate system with one fibre direction.

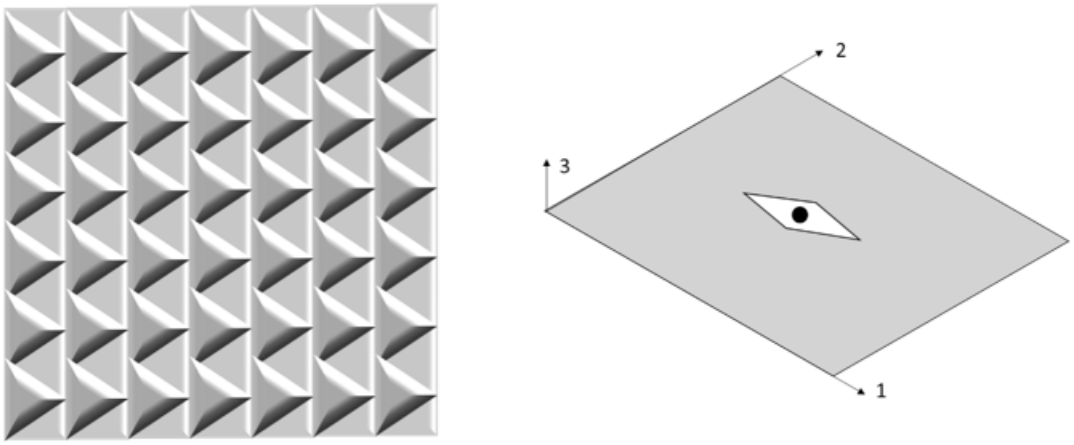

a) b)

Figure 9. a) Scanning for NCF, b) Discretization

Macro mechanical load-dislocation curve

Figure 10 demonstrates how closely the projected elastic factor macro mechanical load-dislocation graph matches the experimental findings. Table 5 shows the results of the macro mechanical load-dislocation graph. Even once fibre deterioration (FD) begins in the model, progressive degradation is extremely accurately reproduced. The model's ultimate degradation is prevented, most likely as a result of an inadequate isotropic destruction composition.

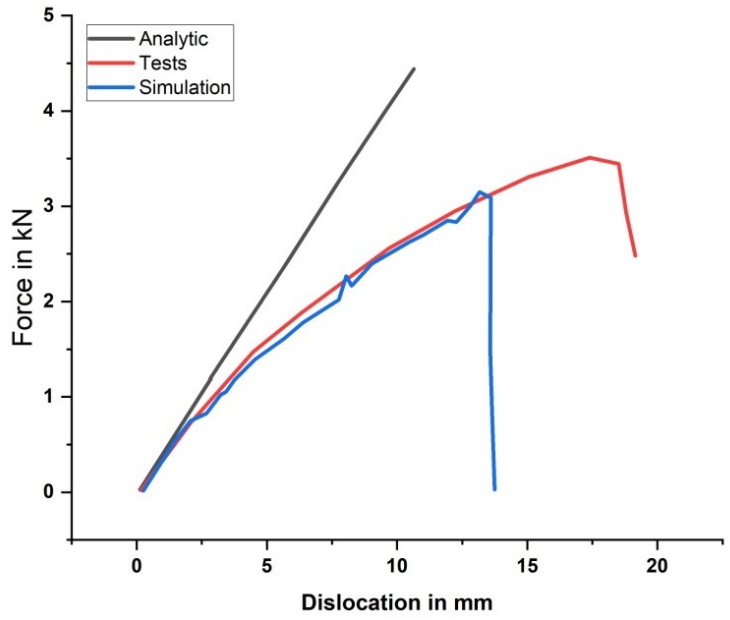

Figure 10. Load-dislocation

Table 5. Results of load-dislocation

Force	Dislocation		
	Analytic	Tests	Simulation
5	2	1.5	1.2
10	4	2.5	2
15	-	3	-
20	-	2	-

To validate the multi-scale method, a three-point bend testing for thickness NCF specimens was generated and compared for experimental results with DLR's Braunschweig. Figure 11 shows the specimens having 2 holes. The application comprises 10 non-crimp fabrics and measures 10 mm thick and 25 mm broad. Stacking sequences are $[0^0/45^0/90^0/45^0//\ 45^0/90^0/45^0/0^0]_5$. This load were applied displacement-driven, with a maximal deflection of 20 mm. To reduce computing effort, one-fourth of the framework is discretized utilizing just symmetrical boundary conditions. Figure 12 illustrates finite element meshes with 158,800 elements (approx. 105, 15, 100) as well as the boundary conditions applied.

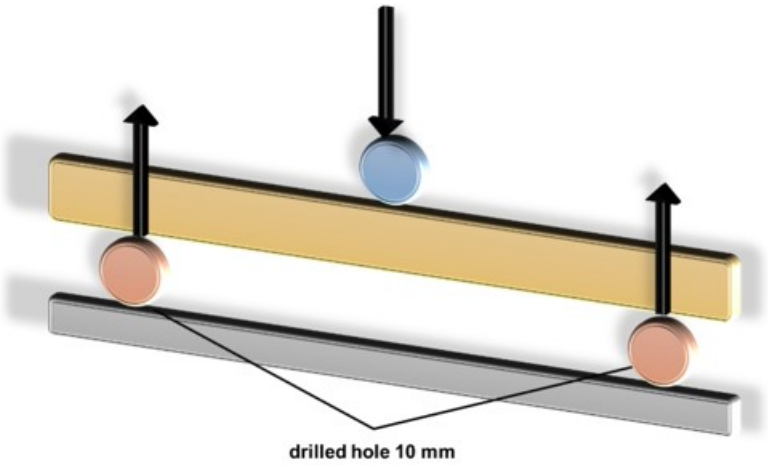

Figure 11. Three-point bend testing

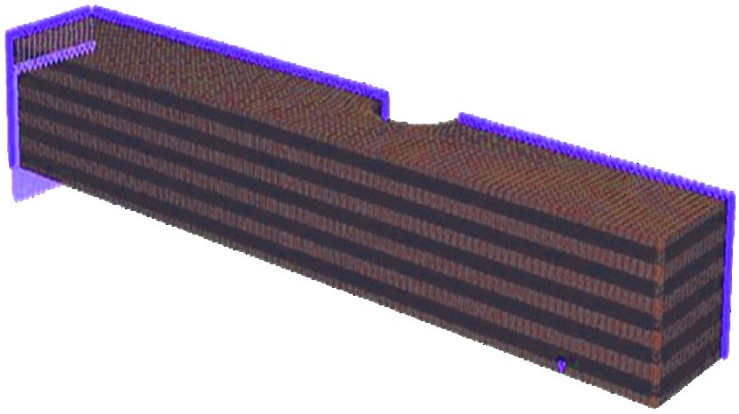

Figure 12. Finite element meshes with three-point bend testing

Macro mechanical rigidity-dislocation curve

The macro mechanical rigidity-dislocation curve is shown in Figure 13. The inter-fibre degradation (IFD) projections made by the proposed softening formulation are accurate and accurately represented as degradation beginning. Although both the initiation of FD in the transverse direction and continuous degradation after IFD are properly predicted, only the forecasting of FF has to be enhanced due to an underestimation of the research's overall strength. Table 6 shows the macro mechanical rigidity-dislocation curve.

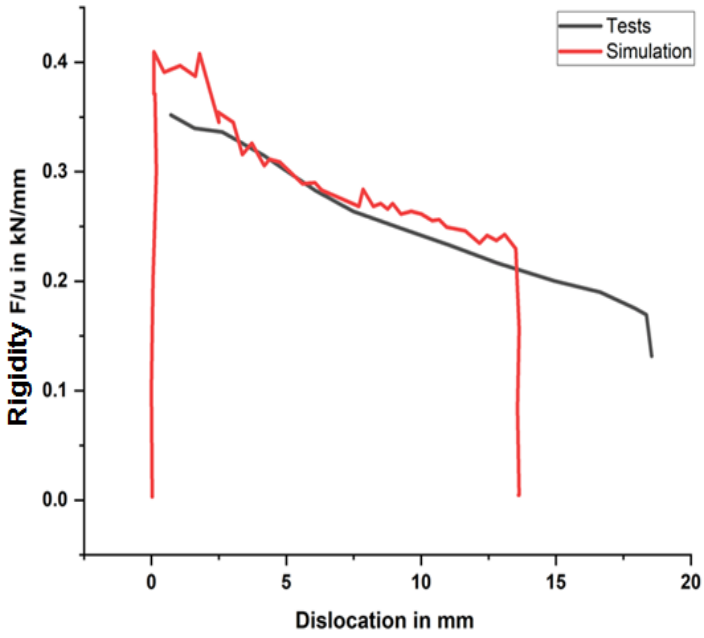

Figure 13. Rigidity-dislocation

Table 6. Results of rigidity-dislocation

Strain	Rigidity-dislocation	
	Tests	Simulation
5	0.28	0.30
10	0.25	0.28
15	0.20	,0.0

CONCLUSION

This study presents a multi-parameter (MP) approach that emphasizes the usage of suitable material and softening concepts to deal with substance nonlinearities that have primarily been neglected up to this point. Yet, a comprehensive explanation of composite durability must take into account the textile material's nonlinearity. To reduce mesh constraints that arise while simulating softening, a normalization technique based on the strain power flow rate is also used. The MP algorithm uses micro- and mid-scale component units. As the mid-structural element is mostly made up of fibre strands, which may be thought of as composites, unidirectional laminate performance is significant in this setting. As a result, the nonlinear unidirectional hybrid behaviour and power may also be determined using this MP approach. If information is accessible, the findings of the virtual assessments are contrasted with those from experiments. To demonstrate the effectiveness of the method, material types, degradation criteria, and softening formulas, a macro-scale case is lastly constructed. Since it operates consistently and provides more options, the MP analysis may both support and replace empirical experiments. It allows for the evaluation of single layers inside a textile layer and subsequently enables it to analyze textile

materials on a layer basis, which is very advantageous during the development stage. The MP analysis for textile fabrics demonstrated the extraordinary stress and strain properties during transversal along with in-plane shear. Energy normalization decreased mesh dependency, while static features were unimportant during compaction. The mid-mechanical unit's curves for stress and strain demonstrated their linear elastic properties till deterioration with transversal compression as well as plastic deflections during shears. The macro-mechanical load dislocation along with rigidity dislocation curves closely corresponded to the experimental results, validating a multi-scale technique. Certain simplifications are frequently added to simulations to make them computationally possible, such as ignoring manufacturing flaws or environmental conditions. In real-world applications, these simplifications could make it more difficult for the model to accurately represent the full complexity of the material behaviour. Further research could concentrate on improving simulations through the incorporation of environmental elements and the resolution of manufacturing flaws, hence increasing model accuracy and practical representation.

Author Contributions

Conceptualization – Peng Y; Methodology – Min Y, Peng Y; Formal analysis – Dang W, Shi H; Investigation – Liu Z; Resources – Liu Z; writing-original draft preparation – Peng Y, Min Y; writing-review and editing – Peng Y, Min Y; visualization – Dang W; supervision – Liu Z. All authors have read and agreed to the published version of the manuscript.

Conflicts of Interest

The authors declare no conflict of interest.

Acknowledgement

The Digital Reform of "Intangible Cultural Heritage" Inheritance Education of Clothing Majors in Hunan Colleges and Universities (HNJG-2022-1158), and The Innovation and Development of Hunan Huayao Cross-stitch Art Under The Trend of Digital Technology (XSP21YBC421).

REFERENCES

[1] Huang R, Zhang S, Zhang W, Yang X. Progress of zinc oxide-based nanocomposites in the textile industry. IET Collaborative Intelligent Manufacturing. 2021; 3(3):281–289. https://doi.org/10.1049/cim2.12029

[2] Nizio KD, Ueland M, Stuart BH, Forbes SL. The analysis of textiles associated with decomposing remains as a natural training aid for cadaver-detection dogs. Forensic Chemistry. 2017; 5:33–45. https://doi.org/10.1016/j.forc.2017.06.002

[3] Anbalagan A, Sundarsingh EF, Ramalingam VS, Samdaria A, Gurion DB, Balamurugan K. Realization and Analysis of a Novel Low-Profile Embroidered Textile Antenna for Real-time Pulse Monitoring. IETE Journal of Research. 2020; 68(6):4142-4149. https://doi.org/10.1080/03772063.2020.1787877

[4] Lee M, Mata-Falcón J, Kaufmann W. Analysis of the tension chord in the flexural response of concrete elements: Methodology and application to weft-knitted textile reinforcement. Engineering Structures. 2022; 261:114270. https://doi.org/10.1016/j.engstruct.2022.114270

[5] Zapata F, Ortega-Ojeda FE, García-Ruiz C. Forensic examination of textile fibres using Raman imaging and multivariate analysis. Spectrochimica Acta Part A: Molecular and Biomolecular Spectroscopy. 2022; 268:120695. https://doi.org/10.1016/j.saa.2021.120695

[6] Jasińska I. The Algorithms of Image Processing and Analysis in the Textile Fabrics Abrasion Assessment. Applied Sciences. 2019; 9(18):3791. https://doi.org/10.3390/app9183791

[7] Monirujjaman Khan M, Islam K, Alam Shovon MN, Masud M, Baz M, AlZain MA. Various Textiles-Based Comparative Analysis of a Millimeter Wave Miniaturized Novel Antenna Design for Body-Centric Communications. International Journal of Antennas and Propagation. 2021; 2021:2360440. https://doi.org/10.1155/2021/2360440

[8] He W, Wang C, Wang H, Jian M, Lu W, Liang X, et al. Integrated textile sensor patch for real-time and multiplex sweat analysis. Science Advances. 2019; 5(11). https://doi.org/10.1126/sciadv.aax0649

[9] Patel DK, Waas AM, Yen CF. Compressive response of hybrid 3D woven textile composites (H3DWTCs): An experimentally validated computational model. Journal of Mechanics and Physics of Solids. 2019; 122:381–405. https://doi.org/10.1016/j.jmps.2018.08.018

[10] Mendes Paim AA, de Andrade MC, Steffens F. The use of textile materials for respiratory protection in times of pandemics: a systematic review and analysis. Research Journal of Textile and Apparel. 2023. https://doi.org/10.1108/rjta-04-2022-0041

[11] Géczy A, Havellant G, Bátorfi R, Skwarek A, Dušek K, Bušek D, et al. Filtering Efficiency of Sustainable Textile Materials Applied in Personal Protective Face Mask Production during Pandemic. Materials. 2023; 16(3):903. https://doi.org/10.3390/ma16030903

[12] Krifa M. Electrically Conductive Textile Materials—Application in Flexible Sensors and Antennas. Textiles. 2021; 1(2):239–257. https://doi.org/10.3390/textiles1020012

[13] Onggar T, Kruppke I, Cherif C. Techniques and Processes for the Realization of Electrically Conducting Textile Materials from Intrinsically Conducting Polymers and Their Application Potential. Polymers. 2020; 12(12):2867. https://doi.org/10.3390/polym12122867

[14] Atanasova D, Staneva D, Grabchev I. Textile Materials Modified with Stimuli-Responsive Drug Carrier for Skin Topical and Transdermal Delivery. Materials. 2021; 14(4):930. https://doi.org/10.3390/ma14040930

[15] Bartkowiak G, Dąbrowska A, Greszta A. Development of Smart Textile Materials with Shape Memory Alloys for Application in Protective Clothing. Materials. 2020; 13(3):689. https://doi.org/10.3390/ma13030689

[16] Machnowski W, Wąs-Gubała J. Evaluation of Selected Thermal Changes in Textile Materials Arising in the Wake of the Impact of Heat Radiation. Applied Sciences. 2021; 11(15):6989. https://doi.org/10.3390/app11156989

[17] Remigijus Ivanauskas, Ingrida Ancutienė, Daiva Milašienė, Algimantas Ivanauskas, Asta Bronušienė. Effect of Reducing Agent on Characteristics and Antibacterial Activity of Copper-Containing Particles in Textile Materials. Materials. 2022; 15(21):7623–3. https://doi.org/10.3390/ma15217623

[18] Iliescu BF, Mancasi VN, Dumitru Ilie I, Mancasi I, Costachescu B, Rotariu DI. Design Principle and Proofing of a New Smart Textile Material That Acts as a Sensor for Immobility in Severe Bed-Confined Patients. Sensors. 2023; 23(5):2573. https://doi.org/10.3390/s23052573

[19] Kudzin MH, Mrozińska Z. Biofunctionalization of Textile Materials. 2. Antimicrobial Modification of Poly(lactide) (PLA) Nonwoven Fabricsby Fosfomycin. Polymers. 2020; 12(4):768. https://doi.org/10.3390/polym12040768

[20] Petrova L, Kozlova O, Vladimirtseva E, Smirnova S, Lipina A, Odintsova O. Development of Multifunctional Coating of Textile Materials Using Silver Microencapsulated Compositions. Coatings. 2021; 11(2):159. https://doi.org/10.3390/coatings11020159

[21] Tseghai GB, Malengier B, Fante KA, Nigusse AB, Van Langenhove L. Integration of Conductive Materials with Textile Structures, an Overview. Sensors. 2020; 20(23):6910. https://doi.org/10.3390/s20236910

[22] Shin J, Han YJ, Lee JH, Han MW. Shape Memory Alloys in Textile Platform: Smart Textile-Composite Actuator and Its Application to Soft Grippers. Sensors. 2023; 23(3):1518. https://doi.org/10.3390/s23031518